# Thermodynamics and phase diagrams of layered superconductor/ferromagnet nanostructures

Paul H. Barsic,[1,*] Oriol T. Valls,[1,†] and Klaus Halterman[2,‡]
[1]*School of Physics and Astronomy, University of Minnesota, Minneapolis, Minnesota 55455, USA*
[2]*Physics and Computational Sciences, Research and Engineering Sciences Department, Naval Air Warfare Center, China Lake, California 93555, USA*

(Received 25 August 2006; revised manuscript received 9 November 2006; published 5 March 2007)

We study the thermodynamics of clean, layered superconductor/ferromagnet nanostructures using fully self-consistent methods to solve the microscopic Bogoliubov-deGennes equations. From these self-consistent solutions the condensation free energies are obtained. The trilayer superconductor/ferromagnet/superconductor junction is studied in particular detail: first-order transitions between 0 and $\pi$ states as a function of the temperature $T$ are located by finding where the free energies of the two phases cross. The occurrence of these transitions is mapped as a function of the thickness $d_F$ of the $F$ layer and of the Fermi wave-vector mismatch parameter $\Lambda$. Similar first-order transitions are found for systems with a larger number of layers: examples are given in the seven-layer (three-junction) case. The latent heats associated with these phase transitions are evaluated and found to be experimentally accessible. The transition temperature to the normal state is calculated from the linearized Bogoliubov-deGennes equations and found to be in good agreement with experiment. Thus, the whole three-dimensional phase diagram in $T$, $d_F$, and $\Lambda$ space can be found. The first-order transitions are associated with dips in the transition temperature $T_c$ to the nonsuperconducting state, which should facilitate locating them. Results are also given for the magnetic moment and the local density of states at the first-order transition.

DOI: 10.1103/PhysRevB.75.104502 PACS number(s): 74.45.+c, 74.25.Bt, 74.78.Fk

## I. INTRODUCTION

The investigation of systems involving ferromagnet ($F$) and superconductor ($S$) junctions is an active component of superconductor-based spintronics[1] research. A broad array of interesting effects arises in $S/F$ nanostructures, which opens doors for nanotechnologies and associated devices and applications that may offer benefits beyond current superconducting devices such as standard Josephson junctions. Advances in fabrication techniques permit growth of ferromagnet and superconductor layers in the form of junctions and heterostructures smooth up to the atomic scale.

The arrangement of consecutive $F$ and $S$ layers, as in $SFS$ junctions, results in competition between magnetic and superconducting orderings. Superconducting correlations can leak into the ferromagnet, while spin polarization can extend into the superconductor: these are the now well established $S/F$ proximity effects.[2,3] The phase coherence embodied in the superconducting correlations becomes modified in the $F$ regions. The exchange energy in the ferromagnet shifts the kinetic energies of the quasiparticles constituting the Cooper pairs and, subsequently, a new superconducting state arises whereby the center of mass momentum of the pair is nonzero.[4] This results in a spatially decaying pair amplitude that oscillates over a characteristic length scale much smaller than the superconducting coherence length. The modulating pair amplitude within the magnet indirectly links adjacent $S$ layers, and thus proximity effects in $F$ cause local oscillations in physically relevant single-particle quantities, including the magnetization[5,6] and density of states[7,8] (DOS). Similarly, in the $S$ material, the magnet locally polarizes the superconductor, causing a monotonic decline in the pairing correlations near the interface over an extended region. The associated spin-split Andreev quasiparticle states also lead to interesting local behavior in the DOS and magnetic moment in the superconductor. The nontrivial behavior of the proximity effects in these structures plays a central role in the competition between the magnetic and superconducting orders.

The modification of the superconducting phase coherence due to proximity effects in clean multilayers consisting of one or more successive $SFS$ junctions is particularly striking. On the atomic level, the pair amplitude is a smoothly varying function of the spatial coordinates. Depending on the values of certain parameters (such as $F$ layer width, $d_F$), the damped oscillatory pair amplitude in the $F$ layer may arrange itself in such a manner that is energetically favorable for its sign to change from one of the $S$ layers to the next, yielding a so-called $\pi$ junction, of the kind proposed long ago for Josephson junctions with magnetic impurities[9] and, subsequently, for $SFS$ systems.[10] If the pair amplitude does not change sign between $S$ layers, it is an ordinary or 0 junction. There is a rich and broad parameter space that then enables a certain level of control over the competing magnetic and superconducting orderings, allowing one to increase or diminish the proximity effects that dominate the relative $SFS$ coupling. The actual equilibrium state (0 or $\pi$) is dependent on several variables, including predominantly the $F$ region's material characteristics and the temperature $T$, all of which ultimately determine the pair amplitude modulation in the magnet. A system comprised of a larger number of $SFS$ sequences results in a greater number of possible 0 or $\pi$ junction combinations.

The transitions between 0 and $\pi$ states can be explored through the signatures of a variety of physical parameters. Experimental study of this question has focused primarily on measurements of the critical current $I_c$ (Refs. 11–19) and, thermodynamically, on the critical temperature[20–26] of the transition to the normal state, $T_c$. Evidence of $0 \leftrightarrow \pi$ transitions can be seen in the $SFS$ Josephson coupling,[27] manifesting itself in the vanishing of $I_c$, although higher-order harmonics in the current-phase relationship can modify this.[28,29]

 ©2007 The American Physical Society

There are also damped oscillations in $I_c$ as a function of $d_F$ and exchange energy in the clean[10] and dirty limits.[30,31] These changes in the critical current have been experimentally confirmed.[11–19] Of particular interest is Ref. 17, which demonstrates the robustness of $0 \leftrightarrow \pi$ transitions by providing evidence of switching in samples with interfaces that were not atomically smooth: despite deviations as large as 0.6 nm over 10% of a sample, clear evidence of switching was found. Near $T_c$, and in the diffusive limit, the theory was later extended to include arbitrary interface transparency.[31] Measurements[20–26] as a function of $d_F$ have shown that $T_c$, which is of course smaller than $T_c^0$, the critical temperature for bulk $S$ material, oscillates as a function of $d_F$, confirming theoretical prediction[32–34] based on the semiclassical Usadel equations[35] in the dirty limit. It has been suggested[33,34] that these oscillations in $T_c$ may be correlated with $\pi \leftrightarrow 0$ transitions. Experimental work[11] has corroborated the existence of the $\pi$ state in *SFS* junctions, and the predicted oscillations in several thermodynamic quantities have, in many cases, been found experimentally. Direct evidence of DOS oscillations in bilayers was reported in a tunneling spectroscopy experiment,[36] but not observed[37,38] in other cases where magnetic impurities[39] were present. Such studies give us the valuable insight that the oscillations in these measurable quantities are correlated with $\pi \leftrightarrow 0$ transitions. Ultimately, all such oscillatory phenomena arise from the oscillations in the pair potential at any $F/S$ interface. In this work, we show that there is indeed an intimate relation between the oscillations in $T_c$ as a function of relevant parameters and the transitions from the $\pi$ to the 0 state, and we find good quantitative agreement with experimental data.

Since the possibility of having a particular junction configuration depends fundamentally on the intricate properties of the pair amplitude, the complicated and demanding task of calculating the pair potential, $\Delta(\mathbf{r})$, rigorously and self-consistently becomes absolutely necessary, particularly as the inhomogeneities occur on a microscopic scale. The first step in the self-consistency process often involves an assumed simple piecewise constant form for $\Delta(\mathbf{r})$, which is then iterated through the relevant equations until convergence is achieved. It is not justified to bypass the technical difficulties associated with self-consistency and to use only an assumed form for the pair potential. The final calculated $\Delta(\mathbf{r})$ often deviates significantly, even in overall symmetry, from the assumed form: the self-consistent $\Delta(\mathbf{r})$ has a complicated spatial behavior that can lead to stable states mixing 0- and $\pi$-junction configurations.[40] A self-consistently calculated pair potential minimizes, at least locally, the free energy of the system. To determine whether the calculated state is merely a local minimum of the free energy or the global one, the free energies from all possible self-consistent 0- and $\pi$-junction configurations must be compared with high precision. Recently developed numerical algorithms[40,41] overcome the difficulties that arise in computing the small difference between much larger quantities and enable accurate computation of the differences in the values of the condensation free energy of different minima.

For clean *SFS* junctions, a relevant set of basic parameters to consider includes $d_F$, the exchange energy $h_0$, and $T$. As these parameters vary, the 0- or $\pi$-state free energies may cross at certain points in parameter space, yielding phase transitions. It has been shown[40] that at $T=0$, transitions occur when varying $h_0$, $d_F$, and also the mismatch parameter $\Lambda$, defined as the ratio (see below) of the bandwidths in the $F$ and $S$ regions. Mismatch can induce a transition because at $\Lambda \approx 1$, when the Fermi wave vectors match, the layers couple more strongly, while at small $\Lambda$, the coupling is effectively weaker. If the temperature varies, it is also possible to have a first-order transition between 0- and $\pi$-junction states, as recently shown in both the clean[41] and dirty[42] limits, and also predicted for short-period $F/S$ superlattices.[33] The temperature has been shown to have a pronounced effect on the pair amplitude in the $F$ region of $F/S$ structures,[43] strongly diminishing its magnitude while maintaining its characteristic period of oscillation as $T$ increases. This translates into weaker coupling between adjacent $S$ layers. If the magnet width is such that the junction is near a $0 \leftrightarrow \pi$ transition point at $T=0$, increasing the temperature can result in the critical current of the junction having a nonmonotonic temperature dependence.[27] It has been argued[44] that the transition is discontinuous in clean *SFS* systems with sharp interfaces and arbitrarily large spin polarizations, but that it can be continuous in diffusive systems with modulated barrier thicknesses.[28] A transition can be observed[17] in just a portion of samples with nonuniform thickness. These results indicate that the temperature can be used to switch between a 0 and a $\pi$-state configuration. It is possible to locate regions of parameter space that give the desired transitions using the $T=0$ results as guides, however, the task is still significantly demanding. Such temperature transitions were found to occur in one-junction and three-junction systems for moderate values of $\Lambda$.[41] Thus, a one-junction system was found to have a $0 \rightarrow \pi$ first-order transition as $T$ was lowered, and a $\pi\pi\pi \rightarrow \pi 0 \pi$ transition was found for a three-junction system.[41] In each case, the free energies of a stable state and a metastable state crossed at the transition temperature with differing derivatives, and therefore entropies. The existence of metastable states and an entropy discontinuity are hallmarks of first-order phase transitions. Moreover, the reported latent heats were reported to be within available experimental resolution. It is therefore desirable to systematically study the coexistence of metastable states and the nature of the transition in *SFS* and higher-order multilayer structures.

The main objectives of this paper, therefore, are to map out the regions of parameter space in which the different junction states are stable and to trace the locations of the phase transitions in systems with *SFS* junctions. An extensive sweep of the geometric and material parameters including $d_F$, $\Lambda$, as well as $T$ is performed. To start with, it is important to know which $d_F$ and $\Lambda$ ranges allow more than one self-consistent state at $T=0$. One can then check if a metastable state at low temperature becomes the equilibrium state at higher $T$. By using this procedure, we obtain a complete phase diagram of an *SFS* junction within the relevant region of $(T, \Lambda, d_F)$ space. To accomplish this, we use a method that can accommodate arbitrary values of the above parameters, without recourse to approximations. As discussed above, all calculations involving the pair potential must be performed using fully self-consistent algorithms, starting from the microscopic equations [Bogoliubov-

deGennes (BdG)]. The need for a fully microscopic theory arises because the characteristic period of the pair potential oscillations approaches the atomic scale. For the nanoscale interlayer widths considered here, geometrical oscillations decisively influence the final results.

We present in Sec. II the microscopic equations and the associated notation relevant for systems containing *SFS* junctions. We review the numerical procedures involved in calculating the self-consistent pair potential and quasiparticle spectra, and the method used to calculate the primary thermodynamic quantity, the condensation free energy, $\Delta\mathcal{F}(T)$, from the self-consistent spectrum and pair potential. We also outline a semianalytic method to calculate $T_c$ through the linearized BdG equations. In Sec. III, we show that first-order transitions with measurable latent heat can occur between states containing different numbers of 0 and $\pi$ junctions as the temperature changes. For *SFS* junctions, the transitions we find are from the $\pi$ to the 0 state as $T$ increases, as found in experiment,[17] and occur predominantly in regions where $T_c$ is low. Using the $T_c$ calculated from the linearized theory and the $0 \leftrightarrow \pi$ phase transitions, we obtain the full phase diagram in an extended region of parameter space spanned by $T$, $d_F$, and $\Lambda$. We compare our calculated oscillations in $T_c$ as a function of $d_F$ with reported Nb/Co experimental data[21] and find good agreement.

## II. METHODS

We study slabs of clean $S$ material separated by $F$ layers. We emphasize trilayers consisting of one *SFS* junction and, as a sample of what can generally occur in multilayers, also present results for seven-layer systems consisting of three *SFS* junctions. We follow procedures[6,7,41] used in previous work; we omit here repetition of technical details and confine ourselves to establishing notation. The thickness of the $S$ layers in each *SFS* junction is denoted by $d_S$, and that of the $F$ layers by $d_F$. The seven-layer system consists of three *SFS* junctions stacked together, so that the thickness of the two inner $S$ layers is $2d_S$. The layers are semi-infinite in the directions perpendicular to the interfaces (the $x$-$y$ directions) and the interfaces are sharp. The spatial inhomogeneity is thus confined to the $z$ direction. We assume parabolic bands: in the $x$-$y$ direction $\epsilon_\perp = k_\perp^2/2m$, where $k_\perp$ is the wave vector in the transverse direction.

### A. Self-consistent solutions

We use the microscopic Bogoliubov-deGennes[45] equations to study this inhomogeneous system. Given a pair potential (order parameter) $\Delta(z)$ to be determined self-consistently, the spin-up quasiparticle $[u_n^\uparrow(z)]$ and spin-down quasihole $[v_n^\downarrow(z)]$ amplitudes obey the BdG equations in the form

$$\begin{pmatrix} H - h(z) & \Delta(z) \\ \Delta(z) & -(H + h(z)) \end{pmatrix} \begin{pmatrix} u_n^\uparrow(z) \\ v_n^\downarrow(z) \end{pmatrix} = \epsilon_n \begin{pmatrix} u_n^\uparrow(z) \\ v_n^\downarrow(z) \end{pmatrix}. \quad (2.1)$$

Here, $H = p_z^2/2m - E_F(z) + \epsilon_\perp$ is a single-particle Hamiltonian, where $p_z^2/2m + \epsilon_\perp$ is the kinetic-energy term. We describe the magnetism by an exchange field $h(z)$, which takes the value $h_0$ in the $F$ material and vanishes in $S$. Within the $S$ layers, $E_F(z)$ is equal to $E_{FS}$, the Fermi energy of the $S$ layers measured from the bottom of the band, while in the ferromagnet, we have $E_F(z) = E_{FM}$ so that in the $F$ regions the up and down bandwidths are $E_{F\uparrow} = E_{FM} + h_0$ and $E_{F\downarrow} = E_{FM} - h_0$, respectively. In the seven-layer case, we assume parallel orientation of the magnetization in all $F$ layers. One should not assume that $E_{FM} = E_{FS}$, and we therefore introduce the dimensionless Fermi wave-vector mismatch parameter $\Lambda$ by $E_{FM} \equiv \Lambda E_{FS}$. Usually, one has $\Lambda < 1$. We introduce the dimensionless magnetic strength variable $I$ by $h_0 \equiv E_{FM} I$. The $I = 1$ limit corresponds to the "half-metallic" case. We neglect interfacial scattering. The amplitudes $u_n^\downarrow(z)$ and $v_n^\uparrow(z)$ can be written down from symmetry relations.[45]

The required self-consistency condition for $\Delta(z)$ is

$$\Delta(z) = \frac{g(z)}{2} {\sum_n}' [u_n^\uparrow(z) v_n^\downarrow(z) + u_n^\downarrow(z) v_n^\uparrow(z)] \tanh\left(\frac{\epsilon_n}{2T}\right), \quad (2.2)$$

where here and below the prime indicates a summation over states for which $|\epsilon_n| \leq \omega_D$, where $\omega_D$ is the usual cutoff "Debye" energy and it is understood that the index $n$ includes $k_\perp$ as well as the longitudinal variables. The BCS coupling $g(z)$ is taken to be a constant $g$ in the superconductor and zero in the ferromagnet.

Exact solutions to Eqs. (2.1) and (2.2) must be computed self-consistently. We begin with an assumed form for $\Delta(z)$, and numerically solve[6,7] Eq. (2.1) for every value of $\epsilon_\perp$ to compute $u_n^\uparrow(z)$, $v_n^\downarrow(z)$, and $\epsilon_n$. An expansion of all quantities in terms of sine waves is used[7] so that the wave functions vanish at the outer edges of the sample. They are continuous and have continuous derivatives at the $F/S$ interfaces. The resulting energy spectrum and quasiparticle amplitudes are used in Eq. (2.2) to compute a new $\Delta(z)$. We then feed this new $\Delta(z)$ back into Eqs. (2.1) and repeat this process until the fractional difference between the average of successive solutions for $\Delta(z)$ is less than a threshold value that we take to be $10^{-5}$.

The self-consistent solution for an *SFS* junction can be of the $\pi$ or the 0 type. For a three-junction system, one can encounter four symmetric states (000, $0\pi0$, $\pi0\pi$, and $\pi\pi\pi$, with each symbol corresponding to the state of each junction). When, for a given temperature and set of geometrical and material parameters such as $I$, $d_F$, and $\Lambda$, several[6,7,41] different self-consistent solutions, that is, local minima in the free energy, exist, the stable state must be determined by comparing the condensation free energies of the competing self-consistent states. To evaluate the free energy $\mathcal{F}$ of the self-consistent states, we use the formula from Ref. 46:

$$\mathcal{F}(T) = -2T {\sum_n}' \ln\left[2\cosh\left(\frac{\epsilon_n}{2T}\right)\right] + \frac{1}{d}\int_0^d \frac{\Delta^2(z)}{g(z)} dz, \quad (2.3)$$

where $d$ is the total thickness of the system.

The condensation free energy is defined as $\Delta\mathcal{F}(T) \equiv \mathcal{F}_S - \mathcal{F}_N$, where $\mathcal{F}_S$ is the free energy of the superconducting state and $\mathcal{F}_N$ that of the nonsuperconducting system. We

compute $\mathcal{F}_N$ by setting $\Delta=0$ in Eqs. (2.1) and (2.3). Calculating $\Delta\mathcal{F}(T)$ is a significant numerical challenge: in a bulk superconductor[47] $\Delta\mathcal{F}(0)=-(1/2)N(0)\Delta_0^2$ [where $N(0)$ is the usual density of states and $\Delta_0$ the order parameter for the bulk superconductor at $T=0$], which is several orders of magnitude smaller than $\mathcal{F}_N \propto N(0)\omega_D^2$. Hence, to obtain $\Delta\mathcal{F}$, we must subtract two numerically obtained large quantities in order to extract a difference several orders of magnitude smaller than the terms subtracted. Also, we shall see that the difference in condensation free energies of competing self-consistent states is a small fraction of the condensation free energy of each of them. To obtain sufficiently accurate values of $\Delta\mathcal{F}$ requires therefore a very high degree of precision in calculating $\mathcal{F}_S$ and $\mathcal{F}_N$. This is made more challenging by the need to calculate derivatives of $\Delta\mathcal{F}$ to obtain thermodynamic functions and latent heats.

### B. Calculation of $T_c$: Linearized solution

While the transition temperature $T_c$ from the nonsuperconducting to the superconducting state can be numerically calculated as the temperature at which $\Delta\mathcal{F}$ vanishes, it is much easier to evaluate $T_c$ by treating $\Delta(z)$ as a small parameter and linearizing the equations. In this way, the calculation is nearly entirely analytic. The amplitudes are written as $u_n^{\uparrow}(z)=u_n^0(z)+u_n'(z)$ and $v_n^{\downarrow}(z)=v_n^0(z)+v_n'(z)$ (we have dropped the spin indices for simplicity). The $u_n^0(z)$ and $v_n^0(z)$ terms are computed from the zeroth-order equation, which is obtained by setting $\Delta(z)=0$ in Eq. (2.1). The form of the zeroth-order equation implies that $u_n^0(z)$ and $v_n^0(z)$ are completely decoupled and have distinct energy spectra, denoted by $\epsilon_n^p$ and $\epsilon_n^h$, respectively. Proceeding to calculate the lowest-order corrections, we incorporate quasiparticle coupling through the pair potential matrix. One can then obtain $u_n'(z)$ and $v_n'(z)$ from textbook perturbation formulas. The intermediate sums are, in principle, over the entire zeroth-order spectrum, but as a practical matter it is enough to include in these sums energies $\epsilon_m^p$ and $\epsilon_m^h$ within a few $\omega_D$ of the Fermi level.

We then expand the quasiparticle amplitudes and their first-order corrections in a sine wave basis $\phi_q(z)$, e.g., $u_n^0(z)=\Sigma_q^N u_{qn}\phi_q(z)$, where $\phi_q(z)=\sqrt{2/d}\sin(k_q z)$, with $k_q=q\pi/d$. The range of the sums over $k_q$ is formally infinite, but again it is only necessary to sum up to a wave number $k_N$ with an associated energy a few $\omega_D$ from $E_F$. Inserting these expansions into Eq. (2.2) gives the lowest-order correction to $\Delta(z)$, which we then expand in the $\phi_q(z)$ basis. Upon taking into account the orthogonality of the basis functions, the expanded Eq. (2.2) is then transformed into the matrix equation

$$\Delta_l = \sum_k J_{lk}\Delta_k, \tag{2.4}$$

where the $\Delta_k$ are the expansion coefficients of $\Delta(z)$ in terms of $\phi_k(z)$. One finds after straightforward algebra:

$$J_{lk}=\frac{gN(0)}{4\pi}\int d\epsilon_\perp {\sum_n}' \left[ \sum_m \sum_{pq}^N u_{pn}^0 v_{qm}^0 K_{pql} \frac{\sum_{ij}^N v_{im}^0 u_{jn}^0 K_{ijk}}{\epsilon_n^p-\epsilon_m^h} \tanh\left(\frac{\epsilon_n^p}{2T}\right) + \sum_m \sum_{pq}^N v_{pn}^0 u_{qm}^0 K_{pql} \frac{\sum_{ij}^N u_{im}^0 v_{jn}^0 K_{ijk}}{\epsilon_n^h-\epsilon_m^p} \tanh\left(\frac{\epsilon_n^h}{2T}\right) \right]. \tag{2.5}$$

Here we have used $gK_{ijk}=\int_0^d g(z)\phi_i(z)\phi_j(z)\phi_k(z)dz$. The integral over $\epsilon_\perp$ reflects the dependence of the zeroth-order quasiparticle amplitudes and energies on $\epsilon_\perp$, and the sum over $n$ is here only over longitudinal quantum numbers, with the prime denoting the limitation indicated below Eq. (2.2) on the energies $\epsilon_n^p$ and $\epsilon_n^p$.

The transition temperature can then be found, in analogy with standard procedures,[48,49] by treating Eq. (2.4) as an eigenvalue equation for the matrix $J_{lk}$. At the transition temperature $T_c$, the largest eigenvalue is unity, while if $T>T_c$, all eigenvalues are less than unity. Unlike the free-energy method described in Sec. II A, this procedure does not require an iterative process and only the last step (finding the eigenvalue) must, in practice, be performed numerically. Therefore this method is much more efficient, and it also provides a check on the numerics of our free energy.

### C. Other quantities

From the self-consistent amplitudes and an energy spectrum, we can also calculate other quantities of interest such as the DOS and the magnetization. The local density of states is

$$N(z,\epsilon)=-\sum_\sigma \sum_n \{[u_n^\sigma(z)]^2 f'(\epsilon-\epsilon_n)+[v_n^\sigma(z)]^2 f'(\epsilon+\epsilon_n)\}, \tag{2.6}$$

where $\sigma$ denotes spin and $f'(\epsilon)$ is the first derivative of the Fermi function. One can also omit the sum over $\sigma$ and obtain the spin-dependent DOS.

Similarly, we have the average number density for each spin subband,

$$\langle n_\sigma(z)\rangle = \sum_n \{[u_n^\sigma(z)]^2 f(\epsilon_n)+[v_n^\sigma(z)]^2[1-f(\epsilon_n)]\}. \tag{2.7}$$

This leads to the dimensionless magnetization,

$$M(z) = \frac{\langle n_\uparrow(z)\rangle - \langle n_\downarrow(z)\rangle}{\langle n_\uparrow(z)\rangle + \langle n_\downarrow(z)\rangle}, \tag{2.8}$$

which reduces to $M(z)=[(1+I)^{3/2}-(1-I)^{3/2}]/[(1+I)^{3/2}+(1-I)^{3/2}]$ for bulk $F$ material within our assumptions. This expression is in numerical agreement with our results from Eq. (2.8) in sufficiently thick $F$ layers.

## III. RESULTS

In this section, we present and discuss our results. As explained above, *SFS* trilayers will be emphasized but results for seven-layer systems comprised of three *SFS* junctions will also be given to show that the single-junction results can be generalized to multilayer samples. We will first discuss the results for the thermodynamics and the phase transitions that ensue. This will include a detailed discussion of the phase diagram for the *SFS* trilayer in the most interesting region of the three-dimensional space spanned by $T$, $\Lambda$, and $d_F$. A discussion of the properties of the transition temperature $T_c$ as a function of $d_F$ and a comparison with experiment follow. We will also discuss other quantities of interest, such as the pair amplitude, the density of states, and the magnetization.

### A. Parameters and units

The results presented will be given in terms of convenient dimensionless quantities. We measure all the lengths in units of $k_{FS}^{-1}$, the Fermi wave vector in $S$. We fix $D_S \equiv k_{FS} d_S = 100$ (except as indicated in Sec. III E). We have taken the BCS coherence length $\xi_0$ equal to $d_S$. For $d_S$ of order of or larger than $\xi_0$, our results are only weakly dependent on $d_S$; hence they are applicable to a very wide range of values of this variable, provided $d_S$ is not too small. The dimensionless thickness $D_F \equiv k_{FS} d_F$ of the ferromagnetic layers will be varied over the range of interest, which corresponds to relatively small values, since at large ones the $F/S$ proximity effects are negligible. Similarly, we introduce the notation $Z \equiv k_{FS} z$. The magnetic strength parameter is taken to be $I=0.2$ unless otherwise noted. The effects of varying $I$ are physically similar to those of varying $D_F$, since the pair amplitude oscillations in $F$ are governed[4] by the difference $(k_\uparrow - k_\downarrow)d_F$ between Fermi wave vectors in the spin bands in $F$. The Fermi wave vector mismatch parameter $\Lambda$ is varied over the experimentally relevant range $0.1 \leqslant \Lambda \leqslant 1$. The temperature is measured in units of $T_c^0$, the critical temperature of a bulk sample of the material $S$. We choose $\omega_D/E_{FS}=0.04$; the dimensionless quantities calculated are not sensitive to this choice. Condensation free energies will be given in units of $N(0)\Delta_0^2$, twice the absolute value of the condensation free energy of a bulk superconducting sample of the same total thickness at $T=0$. A dimensionless measure of the latent heats will be given by dividing the corresponding entropy discontinuities by $C_n(T_c^0)$, the specific heat of a sample of the same overall thickness but consisting exclusively of the $S$ material in its normal metal state at $T_c^0$.

We performed several checks of our numerical methods. We verified that the temperature at which the self-consistent condensation free energy goes to zero is, in each case, the same as the transition temperature obtained from the linearized solution to the BdG equations. For a sample with $d_S \gg \xi_0$ and $d_F=0$, we quantitatively recovered the well-established results[47] for the thermodynamics, including the second-order phase transition at $T_c^0$ and the associated specific-heat discontinuity. The spatially averaged DOS computed numerically for this system shows a well-defined gap at energies within $\Delta_0$ of $E_F$ and the characteristic divergence at $E_F \pm \Delta_0$. This test is very severe since our numerical method must necessarily be more accurate for smaller systems, where fewer variables are required. Thus, the ability of our numerical procedures to handle the relatively large systems (over six superconducting correlation lengths thick) considered here is verified. The low-temperature limit was extensively checked in Ref. 6, and it was also previously verified[7] that our methods give the correct thickness dependence of $\Delta(z)$ for a superconducting slab as found in the literature.[50]

### B. Thermodynamics

The possibility of first-order transitions in systems such as those considered here was previously[41] established. A necessary step now, which is preliminary and necessary to the establishment of the phase diagram, is to show that such transitions are widespread over experimentally significant regions of the parameter space. This step also shows how the transitions are, in general, characterized.

In Fig. 1 we show two instances (among many we have studied) of first-order transitions in *SFS* trilayers. The quantity shown is the self-consistent condensation free energy $\Delta\mathcal{F}(T)$ plotted versus reduced temperature $T/T_c^0$. Data points were obtained at $T/T_c^0=0.01$ intervals. In each panel, the free energies of the two competing states are shown. The thermodynamically stable state is the one with the lower free energy. The outstanding feature of these results is that a metastable state exists at all temperatures from zero up to $T_c$ with a first-order phase transition occurring at an intermediate temperature $T=T_x$ (marked by vertical arrows) where the free energies of the two competing states cross. In both cases shown (and all cases where we have encountered such a transition), the $\pi$ state is stable below $T_x$ and the 0 state above. This was also true in the different case discussed in Ref. 41. We have found that the value of $T_x$ changes smoothly with either $D_F$ or $\Lambda$, or *a fortiori*, both, as done in the two panels of this figure. One can see that, at $T_x$, the slopes of the curves for the stable state and the metastable state are different. Thus, this slope (which is a normalized entropy) changes discontinuously as the stable system switches symmetry with temperature.

The slope of the curves approaches zero as $\Delta\mathcal{F}(T) \to 0$, indicating that the transition to the normal state is of second-order. The temperature at which this second-order phase transition occurs, $T_c$, is the temperature at which the lower $\Delta\mathcal{F}(T)$ vanishes. The $T_c$ found this way agrees with the independently calculated $T_c$ using the linearized BdG equations, thus validating the linearization procedure. The inherent finite-size and proximity effects cause $T_c$ to be considerably smaller than $T_c^0$ in all cases.

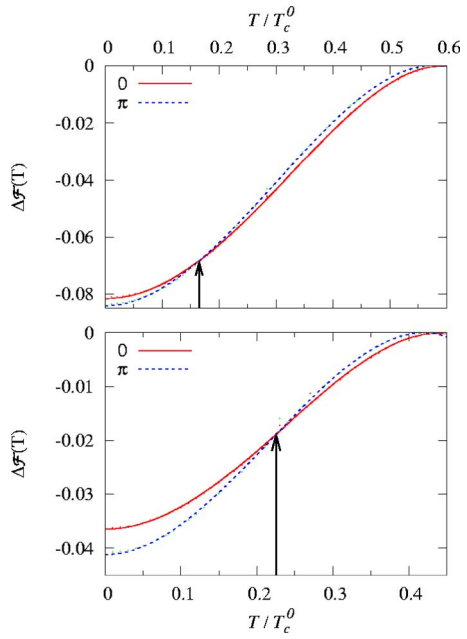


FIG. 1. (Color online) Examples of our results for the normalized (see text) condensation free energy $\Delta\mathcal{F}(T)$ vs temperature for a three-layer *SFS* junction. The different curves are labeled in the legends. In both plots, upon increasing $T$, a $\pi$ to 0 transition occurs at a temperature $T_x$, indicated by the arrows. The top panel shows results for $\Lambda=0.550$ and $D_F=7.1$, with $T_x/T_c^0=0.16$. Bottom panel: $\Lambda=0.650$ and $D_F=5.9$, resulting in $T_x/T_c^0=0.23$.

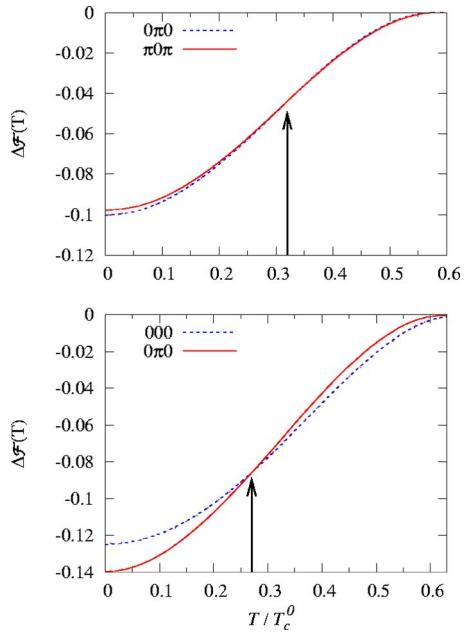


FIG. 2. (Color online) Results for $\Delta\mathcal{F}(T)$ vs reduced temperature (as in Fig. 1) for a seven-layer system. $T_x$ is indicated by the arrows. The different curves are labeled in the legends. The top panel shows a $0\pi0\rightarrow\pi0\pi$ transition for $\Lambda=0.55$ and $D_F=7.9$, at $T_x/T_c^0=0.33$. The bottom panel shows a more pronounced $0\pi0\rightarrow000$ transition for $\Lambda=0.55$ and $D_F=4.75$, with $T_x/T_c^0=0.27$.

Thus, for a range of parameter values including those shown in this figure, the phase-transition behavior is exceptionally rich. That this behavior is widespread is not the same as saying it is universal: in many other regions of $\Lambda$ and $D_F$ parameter space, there is only one self-consistent solution to the BdG equations at $T=0$, while for other ranges, a metastable state is found at low temperature but it never becomes the stable one as $T$ increases. It is only in some regions of parameter space that $0\leftrightarrow\pi$ transitions occur as a function of $T$. This question will be discussed in more detail below.

For the seven-layer case, several different transitions may occur: two cases are shown in Fig. 2. They are both at $\Lambda=0.55$, for different values of $D_F$. In the cases shown, at least two of the four possible metastable states mentioned above exist over the entire temperature range. The states shown in each panel are the two lowest in free energy. Additional states with higher free energy are omitted from the plots. The panels illustrate two different types of phase transitions as $T$ increases: $0\pi0\rightarrow\pi0\pi$ (all three junctions flipping) and $0\pi0\rightarrow000$ (one flip, $\pi\rightarrow0$). A $\pi0\pi\rightarrow\pi\pi\pi$ transition exists also at the same $\Lambda$ for larger $D_F$. Such a transition was previously[41] reported in a different region. As in the three-layer case, the slope of the stable state is discontinuous at $T_x$. Thus, many different first-order transitions occur in multilayer cases. There is an important quantitative difference: $T_x$ varies more slowly with $D_F$ or $\Lambda$, and therefore, the range of parameter values for which such transitions are found is wider. One can expect then that in higher-order multilayers, these phenomena will be even more general.

From the free energy, one can obtain the entire thermodynamics. Figure 3 shows typical thermodynamic functions obtained from the results shown in Fig. 1. Results are shown for two quantities: the dimensionless condensation entropy $S(T)$, defined as the negative derivative of $\Delta\mathcal{F}(T)$ with respect to $T/T_c^0$, and the dimensionless condensation energy $U(T)$, defined as $U(T)\equiv\Delta\mathcal{F}(T)+(T/T_c^0)S(T)$. Results are shown for both the stable and metastable states as a function of reduced temperature. One sees that $S\rightarrow0$ smoothly as $T\rightarrow0$, in agreement with the third law of thermodynamics. This is an important check on the computation. The condensation entropy and energy both vanish at $T_c$. A bold vertical line indicates $T_x$. The free-energy crossings correspond neither to crossings in $S(T)$ nor in $U(T)$. The former indicates that the phase transition is of first order with the associated discontinuity in the entropy being the portion of the bold

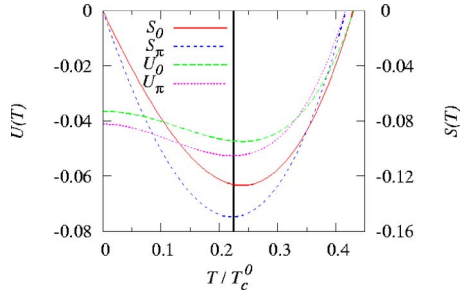


FIG. 3. (Color online) Thermodynamic functions of an *SFS* trilayer. We show the condensation energy and entropy (in dimensionless form, see text) for the parameter set used in the bottom panel of Fig. 1. The meaning of the different curves is indicated in the legend. The location of the first-order transition is marked by the bold vertical line.

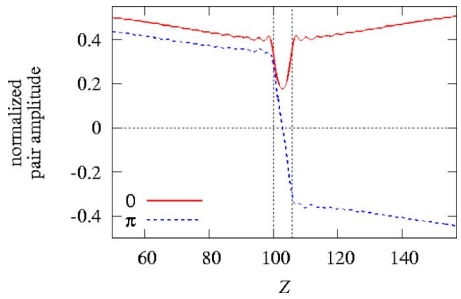


FIG. 4. (Color online) The normalized (see text) pair amplitude for the 0 and $\pi$ states of the *SFS* trilayer, at the crossing point $T_x$, as a function of position $Z \equiv k_{FS} z$. Only the middle portion of the sample is shown. The $F$ layer is delimited by the vertical dotted lines. Results are presented for the parameter set values used in the bottom panel of Fig. 1.

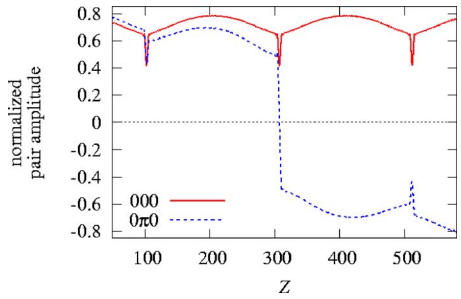


FIG. 5. (Color online) The dimensionless (see text) pair amplitude for the $0\pi0$ and 000 states of the seven-layer system for $\Lambda = 0.55$ and $D_F = 4.75$ at the crossing point $T_x$ as a function of position $Z$. This is the parameter set used in the bottom panel of Fig. 2.

vertical line bounded by the entropy curves. Both the energy and the entropy, therefore, play important roles in the phase transition. The specific heat is not shown, but can be calculated by taking a further derivative. The same behavior is found in all cases for the seven-layer system. Quantitatively, the entropy discontinuities tend to be larger, as we shall see below.

The behavior of the Cooper pair amplitude at the first-order transition is very illuminating. Figure 4 shows, for the *SFS* trilayer at $T = T_x$, this quantity (defined in the usual way as the average of spin-up and spin-down creation operators) normalized to its value in bulk $S$ material at $T = 0$. Results are given versus dimensionless position $Z$. The $F$ region is in the middle, set off by vertical dotted lines, and only small portions of the $S$ regions are shown. The case shown corresponds to the bottom panel in Fig. 1. The absolute value of the pair amplitude is discontinuous at $T_x$: it is slightly larger for the 0 state. This means that the phase transitions are not driven by the pair amplitude. For a bulk superconductor, $\Delta\mathcal{F}$ is proportional to the squared pair potential[47] at $T = 0$ but not[51] at $T > 0$. It is therefore reasonable that this proportionality does not occur in the layered case: the pair amplitudes do not change continuously at $T_x$. The pair amplitude for the three-junction system displays properties very similar to those of a single junction. A representative example, corresponding to $\Lambda = 0.55$ and $D_F = 4.75$, is shown in Fig. 5. The absolute value of the amplitude is again discontinuous at $T_x$. That the seven-layer and three-layer systems have qualitatively similar properties shows that the phenomena we discuss are very general. We can make qualitative predictions for the seven-layer system based on our quantitative (but computationally less demanding) calculations for the three-layer system.

### C. Latent heats

The signature of a first-order phase transition is its latent heat. In Fig. 6, we show results for the dimensionless latent heat $L$, defined as the difference between the entropy of the stable states just above and just below $T_x$ divided by $C_n(T_c^0)$, the specific heat of a normal bulk sample of $S$ material at $T = T_c^0$. This is appropriate because $C_n(T)$ is equal to the entropy in the free-electron model. Results are plotted as a function of $T_x$. Most of the results shown are for a single junction: the crossing temperature is varied by changing $D_F$ for several different values of $\Lambda$, as indicated by the symbols connected by straight segments. The isolated triangles correspond to transitions for the seven-layer system, including those shown in Fig. 2. One of them, corresponding to the bottom panel of Fig. 2, represents a value larger by over a factor of 2 than the upper end of the scale.

The latent heats vanish as $T_x$ approaches 0 or $T_c$, consistent with the smaller condensation entropy of each state in those limits. However, whenever $T_x$ does not approach these limits, the latent heat can exceed 1% of $C_n(T_c^0)$ for one junction, and even more for the three-junction system. Since we give $L$ in units of $C_n$, which is an extensive property, it should be easier to observe these latent heats in larger systems. A value of $L \approx 0.01$ would correspond to picojoules in

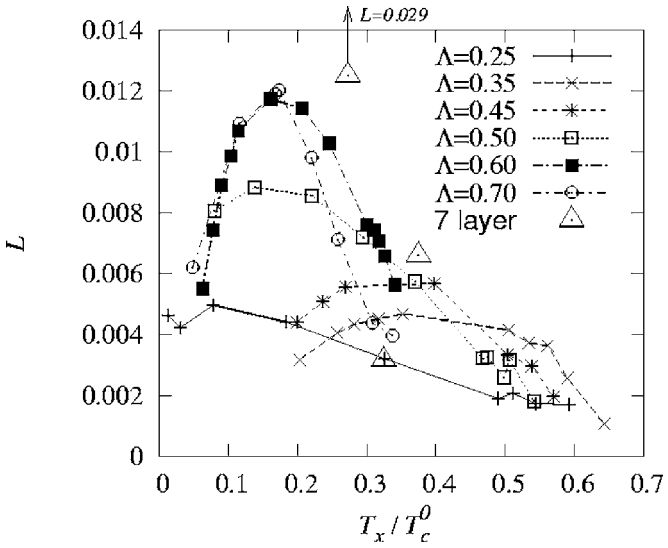


FIG. 6. Latent heat. $L$ is the entropy discontinuity in units of $C_n(T_c^0)$ (see text). It is plotted against the reduced temperature of the first-order phase transition. The symbols joined by lines are for an *SFS* trilayer: the value of $T_x$ is changed along the horizontal axis by varying $D_F$, and from curve to curve by varying $\Lambda$ (see legend). The triangles are for the seven-layer system and include the cases shown in Fig. 2. The vertical arrow attached to the topmost triangle indicates a value $L = 0.029$ (off the scale).

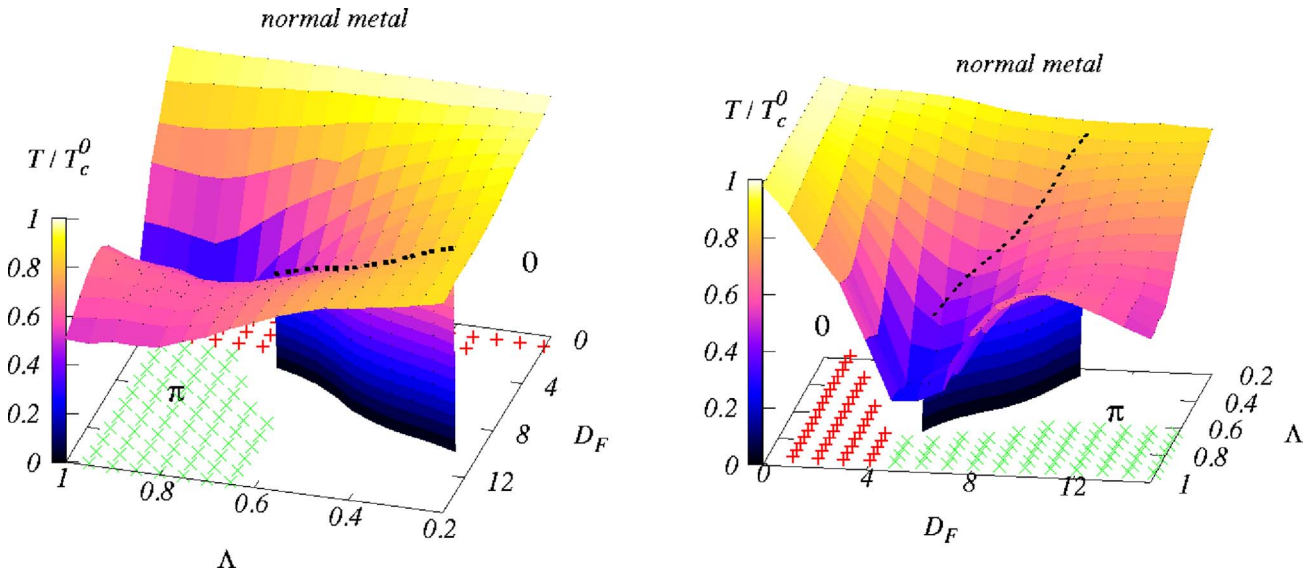


FIG. 7. (Color online) The $(\Lambda, D_F, T)$ phase diagram for the three-layer system. The two panels show different views of the same plot. There are three regions: in those labeled 0 and $\pi$, the 0 and $\pi$ states are, respectively, the equilibrium state, while *normal metal* indicates where the sample is nonsuperconducting. The top surface separates nonsuperconducting and superconducting regions. The fairly vertical sheet marks the temperature transitions between 0 and $\pi$ states. The intersection of the $0-\pi$ and the $T_c$ boundaries is marked by a dotted line. The portion of the $T=0$ plane marked by $\times$ symbols is the range of $(\Lambda, D_F)$ for which only the $\pi$ state exists for all $T$: there is no metastable state of the 0 type. Likewise, in the region marked by + symbols only the 0 state exists. In the portion left blank, solutions of both kinds are possible.

actual samples of relatively small size.[12] Such latent heats can be readily observed via standard techniques used to measure specific and latent heats in films.[52] Even smaller specific heats can be measured using multiple samples: attojoule level results have been reported[53] in electronic systems. We see, therefore, that whenever a first-order transition occurs, the associated latent heat is observable.

### D. Phase diagram

We have seen that in an *SFS* trilayer there are two kinds of phase transitions. First, there are second-order phase transitions from the normal state to a superconducting state of either the 0 or the $\pi$ kind. There are also, at certain ranges of the relevant parameters, first-order transitions between the 0 and $\pi$ superconducting states. As a practical matter, observability of the latter transitions through thermodynamic measurements requires an appreciable difference in condensation energies between the two states. This difference is an oscillatory function of $D_F$ at constant $\Lambda$ and $I$ (see, e.g., Fig. 3 of Ref. 6) with the oscillations becoming damped at large $D_F$, since then, at any $I>0$ the proximity effects are reduced and the 0 and $\pi$ states are degenerate. Hence the most important regions theoretically and experimentally are at relatively small values of $D_F$. As to $\Lambda$, the entire region $\Lambda<1$ is relevant.

Therefore, we have mapped out the entire phase diagram of an *SFS* trilayer in this most relevant region of $(T, \Lambda, D_F)$ space in Fig. 7. As explained above, varying $I$ is equivalent to varying $D_F$, so we use $D_F$ as the more experimentally relevant parameter. We show two views of the phase diagram to aid in the visualization of this three-dimensional figure. There are three regions in this diagram, each representing one of the three possible states: 0 state, $\pi$ state, and normal (not superconducting) state. The crossings $T_x$ are calculated from the free energies, and $T_c$ through the linearization method.

The top sheet shows the superconductor/normal metal transition. As $D_F \to 0$, $T_c/T_c^0$ approaches unity for all $\Lambda$. At small $\Lambda$ the sheet also flattens, since then the Fermi level of the ferromagnet is small compared to $E_{FS}$ so that there is little interaction between the Cooper pairs and the ferromagnet. The finite-temperature $T_x$ transitions between 0 and $\pi$ regions are located at the sheet or "wall" that goes from the $T=0$ plane to the $T_c$ sheet, separating the 0 from the $\pi$ state regions. This wall is, of course, not completely vertical: its deviation from verticality is what causes first-order phase transitions as a function of $T$. On the smaller $D_F$ end, this wall ends because one of the two states becomes unstable: a region of parameter space is entered where only one self-consistent solution exists at any temperature. Coincident with this, as one can see more clearly in the right panel, $T_c$ is sharply reduced: in other words, the condensation energies of both states rise toward zero, with one actually vanishing. Near this region, $T_c$ always has a sharp dip. As one proceeds toward the opposite end of the wall, at larger values of $D_F$, $T_c$ increases and the wall becomes steeper, until it eventually becomes vertical. Beyond that, no transition occurs as a function of $T$: the stable state is the same at all temperatures. Beyond the portion shown, therefore, the wall would become completely vertical and it is not depicted because it would obscure the diagram. It is sufficient to show its behavior in the $T=0$ plane. The crossings at $T=0$ are not thermodynamic phase transitions; they merely indicate a change in the stable

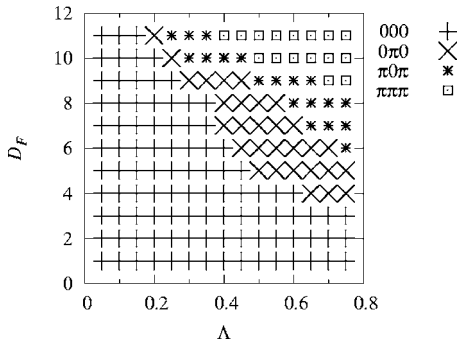


FIG. 8. The $T=0$ plane of the phase diagram for the seven-layer system. The regions in which each of the four possible symmetric states is the stable one are indicated by the symbols in the legend. There are also metastable states at most values of $\Lambda$ and $D_F$.

state as various sample parameters are changed.

Exploration of $T_c$ and $\Delta\mathcal{F}(0)$ for larger values of $D_F$ at several values of $\Lambda$ indicates the existence of other $0-\pi$ boundaries at larger values of $D_F$. Thus, one could extend the phase diagram in that direction, but as previously seen[6] and discussed above, these additional regions are qualitatively similar to the one shown here in detail, and quantitatively less interesting.

Computing a complete three-dimensional phase diagram such as the one in Fig. 7 for a seven-layer system would be very expensive in computational resources and is not necessary. We have already seen, in connection with Fig. 2, that first-order transitions not only occur but are more abundant in such systems. Further evidence is shown in Fig. 8, where we show the zero-temperature plane of the seven-layer phase diagram. A different symbol marks regions where each of the four possible symmetric states is the stable one at very low $T$. The many boundaries between the various states and the presence in many areas of metastable states (not marked) reflect that there may be many first-order phase transitions in the seven-layer system. We can thus infer that even larger structures will have rather intricate and rich phase diagrams. We found that the range of parameter space over which each type of transition persists is much broader than in the three-layer case. For example, for a fixed $\Lambda=0.55$, we observed phase transitions between 000 and $0\pi0$ states for $4.4<D_F<5.0$, transitions between $0\pi0$ and $\pi0\pi$ for $7.75<D_F<8.0$ (see Fig. 2), and transitions between $\pi0\pi$ and $\pi\pi\pi$ for

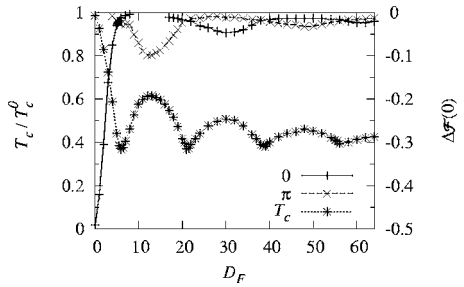


FIG. 9. $T_c$ vs $D_F$ (left scale, $*$ symbols) for $\Lambda=0.70$. Also shown (right scale) are the energies of the 0 and $\pi$ states at $T=0$ ($+$ and $\times$ signs, respectively). Note the correlation between the changes in the stable state at $T=0$ and the dips in $T_c$.

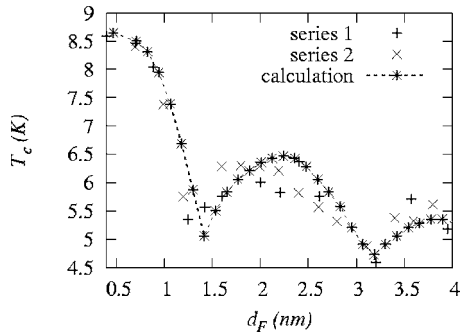


FIG. 10. Calculated values of $T_c$, in good agreement with two reported series (as indicated) of experimental (Ref. 21) data for a Nb/Co system.

$9.0<D_F<9.5$. For a fixed $D_F=10$, the $\pi0\pi\leftrightarrow\pi\pi\pi$ transition exists[41] for $0.35\leqslant\Lambda\leqslant0.50$. We did not search for other transitions at $D_F=10$.

By taking a slice of the phase diagram in Fig. 7 at fixed $\Lambda$, one can discern regular, damped oscillations of $T_c$ with $D_F$. In Fig. 9, we show $T_c$ for $\Lambda=0.70$ over an extended range of $D_F$. It is clear that as $D_F$ is increased, the amplitude of the oscillations decreases. This is in good agreement with experiment, as we shall see in detail below. In addition to $T_c$, this figure shows $\Delta\mathcal{F}(0)$ for the 0 and $\pi$ states. In a bulk superconductor, the ratio of this dimensionless quantity to the reduced transition temperature is $-0.5$, which is confirmed here by our result for the 0 state at $D_F=0$. (The $\pi$ state is unstable, for obvious reasons, in the $D_F\rightarrow0$ limit.) At finite values of $D_F$, this relationship between normalized condensation energy and reduced transition temperature is not strictly obeyed, but there is a qualitative correlation: increases in the absolute value of $\Delta\mathcal{F}(0)$ correspond to increases in $T_c$. The values of $D_F$ at which the stable state at $T=0$ switches between 0 and $\pi$ correspond to sharp dips in $T_c$ in all cases. This has also been seen in connection with Fig. 7 and it indicates that the structure and shape of the oscillations in $T_c$ are strongly correlated with the low-temperature state. Qualitatively, this can be understood as follows: dips in $T_c$ are correlated with smaller values[6] of the absolute value of the pair potential at $T=0$; the superconductivity is, in a sense, "weak," and the difference between the 0 and $\pi$ states becomes smaller. It is then that $T=0$ transitions as a function of $D_F$ can occur. Near these points, it also becomes possible that the stable state may switch as $T$ increases, as we have found. The free-energy data plotted have gaps, notably for the $\pi$ state near $D_F\leqslant4$ and for the 0 state at $8\leqslant D_F\leqslant17$. These values of $D_F$ delimit regions in which the self-consistent calculation resulted in only one state. The free energy of the vanishing state goes continuously to zero at those boundaries. The pair amplitude is also found to go smoothly to zero.

The low-temperature crossings at the many different values of $D_F$ suggest the location of more $0\leftrightarrow\pi$ phase transitions. This is in agreement with the direct observations reported in Ref. 26. Another corroboration of this claim comes from Ref. 17, in which the related parameter which they denote by $I_c$ (the overall critical current of their nonuniform thickness junction) is found to have a significant dip at the

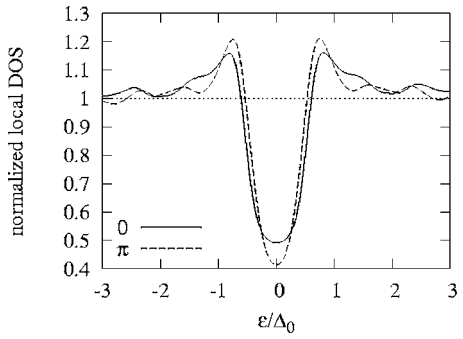


FIG. 11. Density of states at $T_x$ for an *SFS* trilayer. The quantity plotted is the local DOS as defined in Eq. (2.6), averaged over an *S* layer, and normalized to the normal state bulk result in *S*. This is the case shown in the bottom left panel of Fig. 1 ($T_x/T_c^0=0.16$).

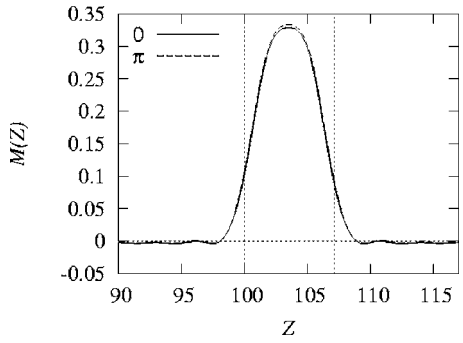


FIG. 12. The dimensionless local magnetization $M(Z)$ for an *SFS* trilayer at $T_x$. Only the central part of the sample is plotted. Results are given for the two nearly coexisting states. The case plotted is the same as in Fig. 11. The vertical dotted lines delimit the *F* region.

$0 \leftrightarrow \pi$ transition temperature. Remarkably, these transitions were observed in Ref. 17 even though their samples did not have layers of uniform thickness. These two experiments and others show that this is an observable and robust phenomenon.

A similar analysis for the seven-layer case showed the same correspondence between $\Delta\mathcal{F}(0)$ and $T_c$. However, the larger number of energy crossings at $T=0$ lead to a closer spacing of energy crossings in $D_F$, causing several local minima in $\Delta\mathcal{F}(0)$ to appear as a single broad minimum. The result was that multiple dips in $T_c$ often merged. In larger systems, the existence of a broad local minimum in $T_c$ may correspond to multiple crossings at low temperature.

### E. Comparison with experiment

Many experimental groups[21–26] have found damped oscillations in $T_c$ as a function of *F* layer thickness. Our calculation also finds these oscillations (see Fig. 9). The agreement with experiment is furthermore quantitative. We show in Fig. 10 a direct comparison of our results to the experimental data for a Nb/Co system.[21,22] In the experiment, the spontaneous magnetization of the Co layer was found to depend on its thickness. This means, in our language, that *I* must be taken as a function of $d_F$ for the purposes of this comparison. To do this, we fitted the spontaneous magnetization reported in Ref. 21 and extracted, at each thickness, the value of *I* from the formula below Eq. (2.8). We took $k_{FS}=1.18$ Å$^{-1}$, which is the textbook value[54] for Nb. The thickness $d_S$ of the experimental samples (400 Å) was nearly equal to the value[55] of $\xi_0$ for Nb. As explained in Sec. III A, our results for $d_S \gtrsim \xi_0$ are nearly independent of $d_S$ as long as $d_S \gg d_F$. We did most of the calculations for this figure at $D_S=k_{FS}\xi_0=100$ and spot checked that the results are the same if one takes both quantities to be 400. A value $\Lambda<1$ is appropriate for the system studied: all values in the range of $0.6<\Lambda<0.7$ give an adequate fit. In the figure, $\Lambda=0.625$. Our fit could be improved by using a $\Lambda$ (i.e., a $k_{FM}$) that varies with thickness, which may be appropriate for thin films. The experimental and theoretical values are in excellent quantitative agreement on the vertical scale, and the damped oscillations are very well aligned in the thickness. Our clean limit theory correctly locates the positions of the minima, and it gives a better fit for these reportedly[22] "high quality" samples than the model employed in Ref. 22.

Comparing Figs. 10 and 9, we conclude that the dips in Fig. 10 must correspond to changes in the stable state at zero temperature. As these changes are, as we have seen, associated with the first-order phase transitions, these dips in $T_c$ may also be associated with first-order phase transitions, in good agreement with what was reported in Ref. 26. This implies that studies of $T_c$ may be a useful tool for experimental discovery of first-order phase transitions and that samples which show dips in $T_c$ are the ones that should be cooled down and studied to locate such phase transitions.

### F. DOS and $M(z)$

Advanced tunneling spectroscopy techniques are a useful experimental tool to measure the local DOS, thus probing the single-particle spectrum. It has been found[6] previously that the local DOS results for 0 and $\pi$ states are different, including a modified subgap structure. In such cases, tunneling spectroscopy could be used to distinguish the states. We now investigate whether the density of states is also a suitable technique in locating phase transitions.

In Fig. 11 we show the DOS, defined as the normalized local DOS [from Eq. (2.6)] averaged over one of the *S* layers, for a typical three-layer system at the temperature where the first-order transition occurs. The case shown is for the same parameters as in the bottom left panel of Fig. 1, with $T_x/T_c^0=0.16$. The energy is normalized to the bulk *S* gap at zero temperature, $\Delta_0$, while the DOS is normalized to its value in a bulk sample of *S* material in its normal state. For both 0 and $\pi$ states, maxima exist near the bulk gap edge, qualitatively reminiscent of the divergence found in a bulk superconductor. The local DOS never quite goes to zero in either state, demonstrating gapless superconductivity induced by the numerous Andreev bound states in the gap. The number of states in the gap is clearly larger for the 0 state and the peak is markedly lower. Although the DOS for both states have some general similarities, the differences that do exist are well within the resolution of current tunneling probes,[36] making the DOS a potentially useful experimental technique in locating the phase transitions or identifying the

stable state in the neighborhood of a transition.

The last quantity we shall briefly describe is the local dimensionless magnetization $M(z)$ as defined in Eq. (2.8). Previous studies[6] indicate that there is little difference between $M(z)$ for the 0 and $\pi$ states at low temperature. In that case, it was found that $M(z)$ was dominated by the exchange parameter $I$ and was rather insensitive to the phase of the superconducting state. There was also little magnetization induced in the $S$ region, as $M(z)$ decayed over the Fermi length scale.[6] To illustrate the effect that temperature has on this trend, we show $M(Z)$ versus the dimensionless length $Z$ at $T=T_x$ in Fig. 12. In the figure, the $F$ region is delimited by vertical dotted lines and only a small portion of the $S$ regions is shown. Consistent with Ref. 6, there is a quick decay and oscillation of $M(Z)$ in the $S$ region. There is a rise in the value of $M(Z)$ to about 0.33 in the center of the $F$ region, which is consistent with the bulk formula below Eq. (2.8) for $I=0.2$. Indeed, as $D_F$ increases, $M(Z)$ flattens to a value that is in good agreement with that estimate. This is not contrary to the experimental results in Ref. 21, for which we modeled the change in the saturation magnetization with $D_F$ by allowing for a $D_F$ dependent $I$, since in that case the magnetic properties (such as the saturation magnetization) of the $F$ layer were experimentally found to depend on $D_F$. Thus, the local magnetization, while interesting for other reasons, is not a good tool for determining the thermodynamically stable state or locating phase transitions.

## IV. CONCLUSION

We have rigorously studied the thermodynamics of clean *SFS* trilayer junctions through self-consistent solutions to the BdG equations, in the clean limit. Building on previous work[41] where $0\leftrightarrow\pi$ transitions in this system were found to be possible, we have computed here the three-dimensional phase diagram of a clean *SFS* junction over an extended and physically relevant region of the space spanned by the parameters $T$, $d_F$, and $\Lambda$. We have found that the transition to the normal state is always of second order, while first-order $\pi\rightarrow 0$ transitions occur, as temperature increases, over a range of $\Lambda$ and $D_F$. Such transitions have been found experimentally. For systems consisting of three such junctions, we have found here that a variety of first-order transitions, involving $0\leftrightarrow\pi$ switching of one or more junctions, occur. The phase transitions were shown to be driven by a delicate balance between the condensation energy and the entropy. The absolute value of the pair amplitude is discontinuous at the first-order transition. Key elements of our approach are an efficient method to accurately compute free energies and a linearization scheme that calculates $T_c$. We have shown that dips in $T_c$ overlap with regions in parameter space where phase transitions exist, which suggest that $T_c$ studies should be useful for experimentally locating first-order phase transitions. We have also calculated the variation of $T_c$ with $d_F$ and found good quantitative agreement with an experimental study[21] of a Nb/Co system. We have demonstrated that the phase transitions will have measurable latent heats, even for relatively small samples, over a broad range of magnet thicknesses. Another experimentally relevant quantity, the DOS, was calculated and deemed a potentially useful tool in locating phase transitions. The local magnetization, however, shows little difference between two states at the first-order transition. The method and results demonstrated here are expected to be applicable to even larger structures.

## ACKNOWLEDGMENT

This work was supported in part by the University of Minnesota Graduate School.

*Electronic address: barsic@physics.umn.edu
†Also at Minnesota Supercomputer Institute, University of Minnesota, Minneapolis, MN 55455. Electronic address: otvalls@umn.edu
‡Electronic address: klaus.halterman@navy.mil

[1] I. Žutić, J. Fabian, and S. Das Sarma, Rev. Mod. Phys. **76**, 323 (2004).
[2] A. F. Andreev, Sov. Phys. JETP **19**, 1228 (1964) [Zh. Eksp. Teor. Fiz. **46**, 1823 (1964)].
[3] A. I. Buzdin, Rev. Mod. Phys. **77**, 935 (2005).
[4] E. A. Demler, G. B. Arnold, and M. R. Beasley, Phys. Rev. B **55**, 15174 (1997).
[5] V. N. Krivoruchko and E. A. Koshina, Phys. Rev. B **66**, 014521 (2002).
[6] K. Halterman and O. T. Valls, Phys. Rev. B **69**, 014517 (2004).
[7] K. Halterman and O. T. Valls, Phys. Rev. B **65**, 014509 (2001).
[8] A. Buzdin, Phys. Rev. B **62**, 11377 (2000).
[9] L. N. Bulaevskii, V. Kuzii, and A. Sobyanin, Pis'ma Zh. Eksp. Teor. Fiz. **25**, 314 (1977) [JETP Lett. **25**, 290 (1977)].
[10] A. I. Buzdin, L. N. Bulaevskii, and S. V. Panyukov, Pis'ma Zh. Eksp. Teor. Fiz. **35**, 147 (1982) [JETP Lett. **35**, 178 (1982)].
[11] W. Guichard, M. Aprili, O. Bourgeois, T. Kontos, J. Lesueur, and P. Gandit, Phys. Rev. Lett. **90**, 167001 (2003).
[12] V. V. Ryazanov, V. A. Oboznov, A. Y. Rusanov, A. V. Veretennikov, A. A. Golubov, and J. Aarts, Phys. Rev. Lett. **86**, 2427 (2001).
[13] H. Sellier, C. Baraduc, F. Lefloch, and R. Calemczuk, Phys. Rev. Lett. **92**, 257005 (2004).
[14] S. M. Frolov, D. J. Van Harlingen, V. A. Oboznov, V. V. Bol'ginov, and V. V. Ryazanov, Phys. Rev. B **70**, 144505 (2004).
[15] B. Jin, G. Su, and Q. R. Zheng, J. Appl. Phys. **96**, 5654 (2004).
[16] M. V. Milošević, G. R. Berdiyorov, and F. M. Peeters, Phys. Rev. Lett. **95**, 147004 (2005).
[17] S. M. Frolov, D. J. Van Harlingen, V. V. Bolginov, V. A. Oboznov, and V. V. Ryazanov, Phys. Rev. B **74**, 020503(R) (2006).
[18] T. Kontos, M. Aprili, J. Lesueur, F. Genêt, B. Stephanidis, and R. Boursier, Phys. Rev. Lett. **89**, 137007 (2002).
[19] V. A. Oboznov, V. V. Bol'ginov, A. K. Feofanov, V. V. Ryazanov,

and A. I. Buzdin, Phys. Rev. Lett. **96**, 197003 (2006).
[20] V. L. Pokrovsky and H. Wei, Phys. Rev. B **69**, 104530 (2004).
[21] Y. Obi, M. Ikabe, T. Kubo, and H. Fujimori, Physica C **317-318**, 149 (1999).
[22] Y. Obi, M. Ikebe, and H. Fujishiro, Phys. Rev. Lett. **94**, 057008 (2005).
[23] J. S. Jiang, D. Davidović, D. H. Reich, and C. L. Chien, Phys. Rev. Lett. **74**, 314 (1995).
[24] J. S. Jiang, D. Davidović, D. H. Reich, and C. L. Chien, Phys. Rev. B **54**, 6119 (1996).
[25] Th. Mühge, N. N. Garif'yanov, Yu. V. Goryunov, G. G. Khaliullin, L. R. Tagirov, K. Westerholt, I. A. Garifullin, and H. Zabel, Phys. Rev. Lett. **77**, 1857 (1996).
[26] V. Shelukhin, A. Tsukernik, M. Karpovski, Y. Blum, K. B. Efetov, A. F. Volkov, T. Champel, M. Eschrig, T. Löfwander, G. Schön, and A. Palevski, Phys. Rev. B **73**, 174506 (2006).
[27] Z. Radović, N. Lazarides, and N. Flytzanis, Phys. Rev. B **68**, 014501 (2003).
[28] A. Buzdin, Phys. Rev. B **72**, 100501(R) (2005).
[29] M. Houzet, V. Vinokur, and F. Pistolesi, Phys. Rev. B **72**, 220506(R) (2005).
[30] A. I. Buzdin and M. Yu. Kuprianov, Pis'ma Zh. Eksp. Teor. Fiz. **53**, 308 (1991) [JETP Lett. **53**, 321 (1991)].
[31] A. Buzdin and I. Baladié, Phys. Rev. B **67**, 184519 (2003).
[32] A. I. Buzdin and M. Yu. Kupriyanov, JETP Lett. **52**, 487 (1990).
[33] Z. Radović, M. Ledvij, L. Dobrosavljević-Grujić, A. I. Buzdin, and J. R. Clem, Phys. Rev. B **44**, 759 (1991).
[34] B. Krunavakarn and S. Yoksan, Physica C **440**, 25 (2006).
[35] K. D. Usadel, Phys. Rev. Lett. **25**, 507 (1970).
[36] T. Kontos, M. Aprili, J. Lesueur, and X. Grison, Phys. Rev. Lett. **86**, 304 (2001).
[37] S. Reymond, P. SanGiorgio, M. R. Beasley, J. Kim, T. Kim, and K. Char, Phys. Rev. B **73**, 054505 (2006).
[38] L. Crétinon, A. K. Gupta, H. Sellier, F. Lefloch, M. Fauré, A. Buzdin, and H. Courtois, Phys. Rev. B **72**, 024511 (2005).
[39] M. Fauré, A. I. Buzdin, A. A. Golubov, and M. Yu. Kupriyanov, Phys. Rev. B **73**, 064505 (2006).
[40] K. Halterman and O. T. Valls, Phys. Rev. B **70**, 104516 (2004).
[41] P. H. Barsic, O. T. Valls, and K. Halterman, Phys. Rev. B **73**, 144514 (2006).
[42] S. Tollis, Phys. Rev. B **69**, 104532 (2004).
[43] K. Halterman and O. T. Valls, Phys. Rev. B **66**, 224516 (2002).
[44] J. Cayssol and G. Montambaux, Phys. Rev. B **71**, 012507 (2005).
[45] P. G. de Gennes, *Superconductivity of Metals and Alloys* (Addison-Wesley, Reading, MA, 1989).
[46] I. Kosztin, Š. Kos, M. Stone, and A. J. Leggett, Phys. Rev. B **58**, 9365 (1998).
[47] M. Tinkham, *Introduction to Superconductivity*, 2nd ed. (Dover, New York, 2004).
[48] P. B. Allen and R. C. Dynes, Phys. Rev. B **12**, 905 (1975).
[49] K. Levin and O. T. Valls, Phys. Rev. B **17**, 191 (1978).
[50] B. P. Stojković and O. T. Valls, Phys. Rev. B **49**, 3413 (1994); **50**, 3374 (1994), and references therein.
[51] See, for example, A. L. Fetter and J. D. Walecka, *Quantum Theory of Many-Particle Systems* (McGraw-Hill, New York, 1971), p. 451.
[52] C. C. Huang (private communication).
[53] O. Bourgeois, S. E. Skipetrov, F. Ong, and J. Chaussy, Phys. Rev. Lett. **94**, 057007 (2005).
[54] See Neil W. Ashcroft and N. David Mermin, *Solid State Physics* (Brooks-Cole, Belmont, MA, 1976), p. 38.
[55] See T. P. Orlando and K. A. Devlin, *Foundations of Applied Superconductivity* (Addison-Wesley, Reading, MA, 1991), p. 575.